Wiley
International Journal of Energy Research
Volume 2025, Article ID 2931509, 16 pages
https://doi.org/10.1155/er/2931509

WILEY

*Research Article*

# Alternative Control Schemes of Pelton Turbines to Increase the Integration of Variable Renewable Energy Sources

**José Ignacio Sarasua Moreno**,[1] **Ana Fernández-Guillamón**,[2,3] **David Carracedo Esteban**,[1] **and Guillermo Martínez-Lucas**[1]

[1]*Department of Hydraulic, Energy and Environmental Engineering, Universidad Politécnica de Madrid, C/Profesor Aranguren 3, Madrid 28040, Spain*
[2]*Department of Applied Mechanics and Projects Engineering, Universidad de Castilla-La Mancha, Avenue de España, s/n, Albacete 02071, Spain*
[3]*Faculty of Engineering, Distance University of Madrid (UDIMA), C/Coruña, km 38500, Collado Villalba, Madrid 28400, Spain*

Correspondence should be addressed to Ana Fernández-Guillamón; ana.fguillamon@uclm.es

Received 25 February 2025; Revised 9 July 2025; Accepted 29 July 2025

Academic Editor: Saleh N. Al-Saadi



This paper proposes innovative control schemes for Pelton turbines to improve frequency regulation in isolated power systems with high penetration of variable renewable energy sources (vRESs). Traditionally, Pelton turbine deflectors are used as safety mechanisms; however, this study explores their potential for continuous frequency regulation, alongside the conventional needle control. The proposed strategies, including a deflector-based control and a mixed control (combining both injector as well as deflector actions), aim to address the limitations of traditional methods. The results obtained from dynamic model simulations demonstrate significant improvements in system performance and stability compared with the traditional needle-based control. In particular, the mixed control strategy achieves a balanced solution, minimizing frequency deviations, reducing water losses, and maximizing renewable energy integration. These findings highlight the potential of advanced turbine control to optimize the operation of isolated power systems and support the transition to sustainable energy systems.

**Keywords:** deflector-based control; frequency regulation; isolated systems; Pelton turbines; renewable integration

## 1. Introduction

The nonstop increase in electrical consumption, together with the increasingly notorious environmental effects of the emissions due to conventional power plants, has caused the evolution of electrical grids worldwide [1]. As a consequence, most countries are replacing their polluting power plants (coal-, oil-, gas-, and nuclear-based) with variable renewable energy sources (vRESs; mainly wind and photovoltaic installations) [2]. Among them, wind energy is a cost-effective and sustainable vRES that many countries are adopting to increase clean energy in their grids [3]. However, this high wind penetration has raised several problems in terms of power systems' stability, as it depends on a natural and uncontrollable resource and is electrically decoupled from the grid by power converters [4]. In fact, as the integration of wind increases, power systems have lower inertia, and the power fluctuations due to the stochastic process of the turbulent fluctuations in wind speed may reduce the power quality of the electrical grid [5, 6].

Isolated power systems face unique challenges with high levels of wind integration, due primarily to their limited connectivity and smaller grid size compared to interconnected systems [7]. Without the stabilizing influence of external power systems, these isolated grids are more susceptible to fluctuations, which can lead to significant issues in maintaining frequency and voltage stability [8]. The intermittent nature of wind introduces an added layer of complexity, forcing isolated systems to rely on a combination of fast-responding backup resources or energy storage systems to stabilize the grid [9, 10].

When doing the electrical transition planning, the characteristics of each power plant must be considered: depending on them, the power plants can play different roles within the power system [11]. One of the main aspects of power plants is their flexibility, where gas and hydroelectric power plants are the most effective options [12]. Given their operational flexibility, hydroelectric power plants are supposed to play an increasingly critical role in the future energy landscape, particularly as the transition away from fossil fuels intensifies [13, 14]. Recently, an extensive review of the factors that can affect the flexibility of hydroelectric power plants was carried out [15]. Moreover, hydroelectric power plants have the ability to serve as energy storage capabilities through pumped storage, positioning them as a vital component in achieving a reliable and sustainable electrical system [16].

Currently, there are several isolated power systems with high wind power integration and (pumped storage or not) hydropower plants, which are usually equipped with Pelton turbines. Katsaprakakis et al. [17] analyzed the implementation for the isolated power system of the isles Karpathos and Kasos (Greece), which were initially fueled by 5 diesel engines and a wind power plant. The proposed system kept the wind power plant, but included a pumped storage system with 2 Pelton turbines of 2 MW each to minimize the use of fossil fuels. A medium-sized islanded power system in the European Atlantic region is analyzed in [18, 19]. These authors evaluated the feasibility and impact of integrating a pumped storage hydroelectric power plant into such an isle, reliant on thermal and renewable energy sources (RESs). The proposed hydropower plant included a 7 MW Pelton turbine and 7.5 MW of pumping capacity. Similarly, Sebastián and Nevado [20] examined a wind–hydro isolated microgrid designed for remote autonomous operation, including a hydropower plant with a Pelton turbine, a wind turbine, and a dump load for dissipating excess energy. The microgrid can operate in three modes: hydro-only, wind-only, and wind–hydro, transitioning between them based on power supply and demand. Moreover, the island of Eigg, in Scotland, has a hybrid system consisting of three hydroelectric generators (100, 6, and 5 kW), four wind turbines (6 kW each), and a photovoltaic installation (170 kW), supplying 95% of the demanded electricity on the island [21]. In Spain, one notable case stands out. A hybrid wind and pumped-storage hydropower facility known as Gorona del Viento was commissioned in June 2014 within the El Hierro power system. This pumped-storage plant includes four Pelton units (4 × 2.83 MW), six fixed-speed pumps (6 × 0.5 MW), and two variable-speed pumps (2 × 1.5 MW). In recent years, the importance of this complex power plant has grown within the power system. During the summer of 2019, electric demand was met continuously and solely by RES for a total of 596 h [22].

Pelton turbines are installed in about 20% of hydroelectric power plants [23]. These turbines are suited to the use of very steep waterfalls (between 30 and 1000 m) and relatively small flows (between 0.1 and 11,000 l/s) [24], which means that they are used in power plants with long conduits. The nozzle, which is the organ that regulates the flow rate impinging on the turbine runner, is fitted with a needle valve whose position determines the opening level and, thus, the flow rate [25].

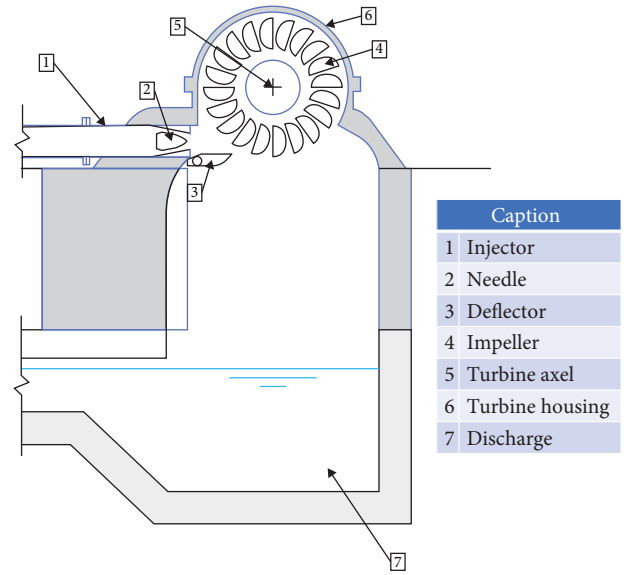


Figure 1: Diagram of Pelton turbine components.

Sudden movements of the injector can cause pressure waves, that is, water hammer, in the penstock [26]. These pressure waves hinder the frequency regulation of the electrical system itself, as has been discussed in several publications [27, 28]. In addition to having an injector, the Pelton turbine also has a deflector. It consists of a metal surface designed to deflect the water jet and prevent it from impacting the cups, as can be seen in Figure 1. The deflector is usually used as a safety feature: when a hydroelectric unit is suddenly shut down, the wicket gate of a reaction turbine is normally closed quickly to prevent overspeed of the runner, which can be very damaging [29]. However, this sudden closure of the wicket gate causes an overpressure (water hammer) in the conduits. In the case of action turbines, such as Pelton turbines, the deflector allows the water jet to be deflected, preventing the water from hitting the cups, that is, avoiding overspeed in the runner without the need to close the nozzle abruptly, and therefore avoiding overpressure in the penstock.

Together with the safety feature, the deflector has sometimes been studied to enhance the frequency regulation of power systems. The works carried out by Johnson et al. [30, 31] described the problems that occur in the Kenai grid (Alaska) when the line connecting it to the main system was damaged; in such a situation, the Kenai grid changed from exporting electricity to being an isolated system, and the Pelton turbines had to drastically reduce their generation. To overcome that, the authors proposed a new control for the turbine deflector, which operated simultaneously with the injectors, eliminating the instabilities caused by the overspeed of the groups. Wang et al. [32] developed a Pelton turbine and governor system dynamic model in association with the characteristics of a deflector overspeed control for a Pelton turbine. Recently [33], sought to counteract the difficulties caused by water hammer in the frequency control of a Pelton turbine, considering a hydropower plant in Austria. This needed to limit the speed of movements in the injector to 3%/s in the power plant studied. To improve the action of the frequency

control, the authors proposed a PID control for the deflector, which could only act by limiting the power when there was an overfrequency. This same proposal was used in [34] by locating the deflector close to the water jet, which allowed the distributor controller to be more energetic, as there was no "bouncing" effect on the frequency.

Thus, the frequency regulation in Pelton turbines can be achieved by using both electromechanical elements: the nozzle and the deflector. The nozzle regulates the water flow through a needle operated by servomotors, as is usually. Additionally, deflector plates, also controlled by servomotors, can divert a portion of the water jet emitted by the nozzle, ensuring that only a specific percentage impacts the runner bowl. This reduces pressure waves and overpressure in the penstock during frequency regulation or plant shutdowns. However, using the deflector instead of the nozzle needle for complete frequency regulation results in a partial or total flow loss, as water continues flowing through the pipe without impacting the runner [35]. Consequently, deflectors are typically employed solely for overspeed scenarios, as justified by the previously published works. To the best of the authors' knowledge, no frequency controller has been proposed so far that includes continuous action of the deflector. This may be due to the fact that using the deflector, either exclusively or partially, for frequency regulation would lead to an excessive loss of water. However, the increasing penetration of vRES, particularly in isolated power systems, provides a new context in which this hybrid control strategy becomes globally efficient despite the associated water losses.

This combined control strategy can be considered analogous to other hybrid control schemes involving hydropower plants and fast storage systems, such as batteries or flywheels. In such schemes, the storage system provides a fast response to frequency deviations, similar to the one that could be delivered by the deflector of a Pelton turbine. For instance, [36] described a hierarchical hybrid frequency control composed of a hydropower plant and a flywheel system. Through a specific algorithm, the flywheels absorb sudden frequency variations, while the hydropower plant manages the state of charge of the flywheels, maximizing overall performance. In the study conducted by Vasconcelos et al. [37], a flywheel system performed proportional control in response to frequency deviations in an isolated power system. In [22], the authors proposed a hybrid frequency control combining a hydropower plant, wind turbines, and flywheels.

Another type of hybrid control comparable to the one proposed here is found in systems where variable-speed wind turbines provide synthetic inertia for frequency regulation. These turbines can quickly inject or absorb active power, much like the deflector of a Pelton turbine, at the cost of the kinetic energy stored in their rotors. In [38], a hybrid control scheme is proposed involving a hydropower plant and a group of wind turbines in an isolated system, whereas [39] addressed the combination actions of a photovoltaic and a wind power plant for frequency control in an isolated system.

This paper proposes a novel approach that incorporates continuous deflector control for both overfrequency and underfrequency regulation. Priority has been given to the ease of implementation of the new controllers by adopting an architecture similar to the existing proportional-integral (PI) controller. This control is particularly valuable for isolated power systems with large RES integration, where the vRES generation can sometimes be limited due to frequency variability, even though the natural resource would be able to provide more electricity [40]. By stabilizing frequency variability, this strategy allows greater vRES integration while maintaining acceptable frequency margins.

To thoroughly evaluate these schemes, a dynamic simulation model was developed in MATLAB Simulink, accurately reflecting an isolated power system that includes a hydroelectric plant with Pelton turbine deflector behavior, among other advanced technologies. The case study presented validates the effectiveness of these control strategies in real-world conditions, demonstrating the model's potential as a valuable tool for optimizing vRES integration and improving system resilience. The rest of the paper is organized as follows: Section 2 describes the developed dynamic model; Section 3 proposes different control schemes for the Pelton turbine, which are applied to the case study described in Section 4; and finally, the conclusions are given in Section 5.

## 2. Dynamic Model

In order to study the proposed frequency control strategies provided by the Pelton turbines using their deflector in an isolated system, an aggregated inertial model is developed in MATLAB Simulink to represent grid frequency variations [41]. This assumption, applicable to isolated power systems, has been previously used both in the electrical system of El Hierro [42] and in the modeling of the Irish electrical system [43]. The considered isolated power system with wind energy penetration, along with the model developed in MATLAB Simulink, consists of a hydroelectric power plant equipped with four Pelton units, a pump station with two variable speed pumps (VSPs) and six fixed speed pumps (FSPs), a wind power plant with five variable speed wind turbines, an automatic generation control (AGC), the equivalent power system, and a frequency-sensitive power demand (Figure 2). The dynamics of transmission lines are considered negligible for grid frequency variations [44]. Furthermore, it is assumed that electromagnetic transients are much faster than other components in the model, and therefore their impact on the system's dynamics can also be disregarded [27].

The equations used to model the hydroelectric power plant (except Pelton units, whose model is detailed in Section 2.1) and the pumping station have been previously employed by the authors [42]. Both the pumping station and the hydroelectric power plant share the upper and lower reservoirs, though each operates through a distinct hydraulic circuit with its own penstock. Given the length of the penstocks, an elastic water column model is necessary to accurately represent their dynamic behavior. The lumped parameter approach has been adapted by the authors to account for the specific characteristics of the penstocks. The modeling strategy yields a system of ordinary differential equations, which can be conceptualized as a sequence of interconnected $\Gamma$-shaped modules. Within this

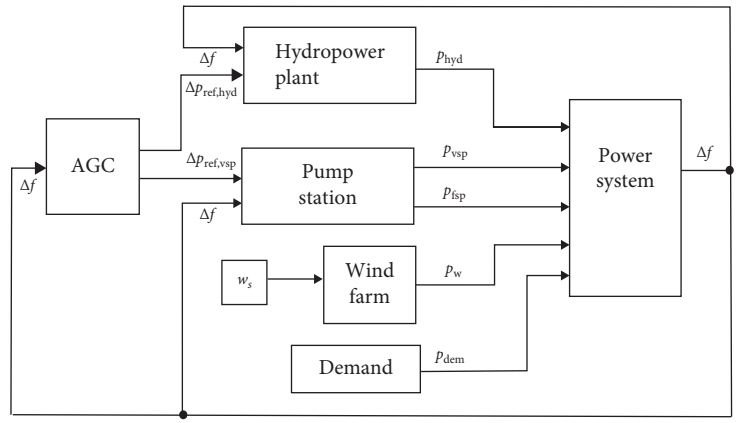


FIGURE 2: Block diagram of the dynamic model.

TABLE 1: Hydropower plant model parameters.

| | | | | | | | |
|---|---|---|---|---|---|---|---|
| $n_t$ | 10 | $\frac{r}{2}$ | 0.0010 | $L$ | 2577 m | $S$ | 0.785 $m^2$ |
| $Q_b$ | 0.5 $m^3/s$ | $H_b$ | 658 m | $T_e$ | 2.16 s | $T_w$ | 0.2542 s |

scheme, the physical properties of the conduit, namely inertia, elasticity, and friction, are distributed proportionally to the segment length $L_e$. The specific configuration and alignment of these $\Gamma$-shaped elements depend on the boundary conditions applied at the pipe's upstream and downstream ends. Accordingly, the governing equations that describe the dynamic behavior of the penstock are given in Equations (1) and (2), where the water starting time $T_w$ is defined by Equation (3). Parameters used in the hydropower plant model are listed in Table 1.

$$\frac{dq_{p,m}}{dt} = \frac{n_t}{T_w}\left(h_m - h_{m+1} - \frac{r}{2n_t}q_{p,m}|q_{p,m}|\right), \tag{1}$$

$$\frac{dh_m}{dt} = n_t\frac{T_w}{T_e^2}\left(q_{p,m} - q_{p,m+1}\right), \tag{2}$$

$$T_w = \frac{L}{gS}\frac{Q_b}{H_b}. \tag{3}$$

Regarding the pump station, the net head for each pump is calculated using Equation (4), while the mechanical power required by the hydraulic machine to elevate the flow is obtained from Equation (5) [45]. Both equations are derived from the characteristic pump curves corresponding to nominal rotational speeds under FSP and VSP operating modes. Hydraulic similarity laws are applied to extrapolate the net head and mechanical power for off-nominal rotational speeds.

$$h_{n,i} = \left(c_{h,i}q_i^2 + b_{h,i}q + a_{h,i}\right)\left(\frac{n_{p,i}}{n_{\text{nom},i}}\right)^2, \tag{4}$$

$$p_{n,i} = \left(c_{p,i}q_i^2 + b_{p,i}q + a_{p,i}\right)\left(\frac{n_{p,i}}{n_{\text{nom},i}}\right)^2. \tag{5}$$

Equation (6) is employed to evaluate the speed deviations of each electrical machine, $n_{p,i}$, as a result of the imbalance between mechanical and electrical torques. This formulation applies to both FSP and VSP cases, with the inertia constant $J_i$ varying accordingly [45] as follows:

$$n_{p,i}\frac{dn_{p,i}}{dt} = \frac{1}{J_i}\left(p_{e,i} - p_{p,i}\right). \tag{6}$$

The electrical power consumed by the fixed-speed asynchronous machines is obtained using Equation (7) as follows:

$$p_{e,i} = \begin{cases} \left(K_{p,p} + K_{p,i}\int dt\right)\left(f - f_{\text{ref}}\right) + p_{e,i}^0 & \text{for } i = 1,\ 8 \\ \dfrac{1 - \frac{n_{p,i}}{f}}{s_{\text{nom}}}\dfrac{N_{\text{syn}}}{N_{\text{nom},i}} & \text{for } i \in [2, 7] \end{cases}. \tag{7}$$

The values of all the parameters used in the pumping station model are provided in Appendix A of [45].

Although all eight electrical machines are asynchronous, units 1 and 8 are equipped with full converters, allowing them to adjust the power they consume. In these units, a PI controller regulates the electrical power drawn from the grid [45].

The wind power plant model, which includes the quantification of the mechanical power produced in the wind turbine from the wind speed as well as both pitch control and torque-based maximum power point tracking control of each variable

Table 2: Wind turbines model parameters.

| | | | | | |
|---|---|---|---|---|---|
| $K_{p\omega}$ | 0.6 | $K_{i\omega}$ | 0.12 | $2H_{\omega}$ | 3.718 s |

speed wind turbine, is derived from [46]. The power extracted from the wind is modeled using Equation (8) as follows:

$$P_{\text{wind}} = \frac{\rho}{2} A_r s_w^3 C_p(\lambda, \beta)\ , \tag{8}$$

where the power coefficient $C_p$ is a fourth-order function of the turbine tip speed ratio $\lambda$ and the pitch angle $\beta$ [47].

Pitch control is a combination of conventional pitch angle control and pitch compensation. The conventional pitch angle control implements a PI control that computes the difference between the rotor and reference rotor speeds [48]. Furthermore, the pitch angle control considers the compensation through a different PI control that computes the difference between the mechanical wind power and maximum rated power for each wind speed [49].

The torque-based maximum power point tracking control controls the rotational speed by regulating the electromagnetic torque, recovering the optimal speed once the frequency transient has subsided. It was considered the simplest controller to make the conclusions more general. Therefore, a PI controller obtains a power reference, $\Delta p_{\omega}$ (Equation (9)) based on the difference between the rotational speed and the optimal rotational speed [50] as follows:

$$\Delta p_{\omega} = \left[K_{p\omega} + K_{i\omega} \int dt\right](\omega - \omega_{\text{ref}}). \tag{9}$$

The total power supplied by the electronic converter will be the sum of the mechanical power initially produced by the wind and the power increment $\Delta p_{\omega}$ that has been previously described.

For the rotor's mechanical model, a single-mass rotor model is employed as expressed in Equation (10), which is sufficient in scenarios where the power converter decouples the generator from the grid [51]. Parameters used in Equations (9) and (10) are listed in Table 2.

$$\frac{d\omega}{dt} = \frac{1}{2H_w} \frac{1}{\omega} (p_w - p_{nc}). \tag{10}$$

Although modern wind turbines are capable of contributing to frequency regulation and inertia emulation [38], this study assumes no such contribution from this generation technology as in other previously published research [52]. In the simulation model, power demand and wind speed are treated as input variables.

System frequency oscillations occur following imbalances between the power supplied by the generating units, that is, hydroelectric units $(p_{\text{hyd}})$ and wind turbines $(p_w)$, and the power demand by the pump station, which includes both fixed-speed pumps $(p_{\text{fsp}})$ and VSPs $(p_{\text{vsp}})$ as well as consumer loads $(p_{\text{dem}})$. The sensitivities of the consumer load to frequency variations are included in the model by means of the parameter $(D_{\text{net}})$. Thus, the frequency variations are formulated in Equation (11) as follows:

$$f\ \frac{df}{dt} = \frac{1}{2\ H_{\text{hyd}}}\ \left(p_{\text{hyd}} + p_w - p_{\text{fsp}} - p_{\text{vsp}} - p_{\text{dem}} - D_{\text{net}} \cdot \Delta f\right). \tag{11}$$

The system's inertia term $(H_{\text{hyd}})$ corresponds to the inertia constant of the hydroelectric units operating at each moment. Wind turbines are connected to the grid through power converters, so they cannot directly provide inertia to the grid.

Frequency control is delineated into two sequential phases. In the initial phase, frequency deviations are rectified by the generation units and VSP by adjusting their power output/input in accordance with the droop assigned to each unit, a process known as primary regulation. In the subsequent phase, the steady-state frequency error resulting from the initial control action is addressed by the AGC, which determines the secondary corrective action. The AGC system is modeled as described in [53]. The total secondary regulation effort ($\Delta RR$) is obtained as indicated in Equation (12) as follows:

$$\Delta RR = -\Delta f\ K_f. \tag{12}$$

$K_f$ is determined according to the ENTSO-E recommendations [54]. This regulation effort is distributed among each $i$ synchronized generating unit as a function of their participation factors ($K_{u,i}$), as expressed in Equation (13) as follows:

$$\Delta p_i^{\text{ref}} = \frac{1}{T_{u,i}} \int \Delta RR\, K_{u,i}\, dt = \frac{-1}{T_{u,i}} \int K_{u,i}\, K_f\, dt\ , \tag{13}$$

where $i$ represents each online generation unit. Note that the participation factors of generating units disconnected from the grid are considered as 0. Consequently, it is assumed that all generating units connected to the power system actively participate in secondary regulation. The participation factors are obtained as a function of the speed droop of each unit [55], being the sum of all participation factors equal to 1.

*2.1. Pelton Units.* Due to the importance of the modeling of the Pelton turbine, the expressions governing its operation are detailed below. Equation (14) [56] gives the relationship between p.u. values of flow $q$, head $h$, and nozzle opening $z$, where $i$ correspond to each online Pelton turbine from 1 to 4. Since there is only one penstock, it is assumed that the head upstream of each turbine is equal.

$$q_i = z_i \sqrt{h}. \tag{14}$$

Equation (15) is used for p.u. shaft torque corresponds to ideal rated conditions, where the absolute fluid speed is twice the runner peripheral speed [26], corresponding $i$ to each online Pelton turbine from 1 to 4 as follows:

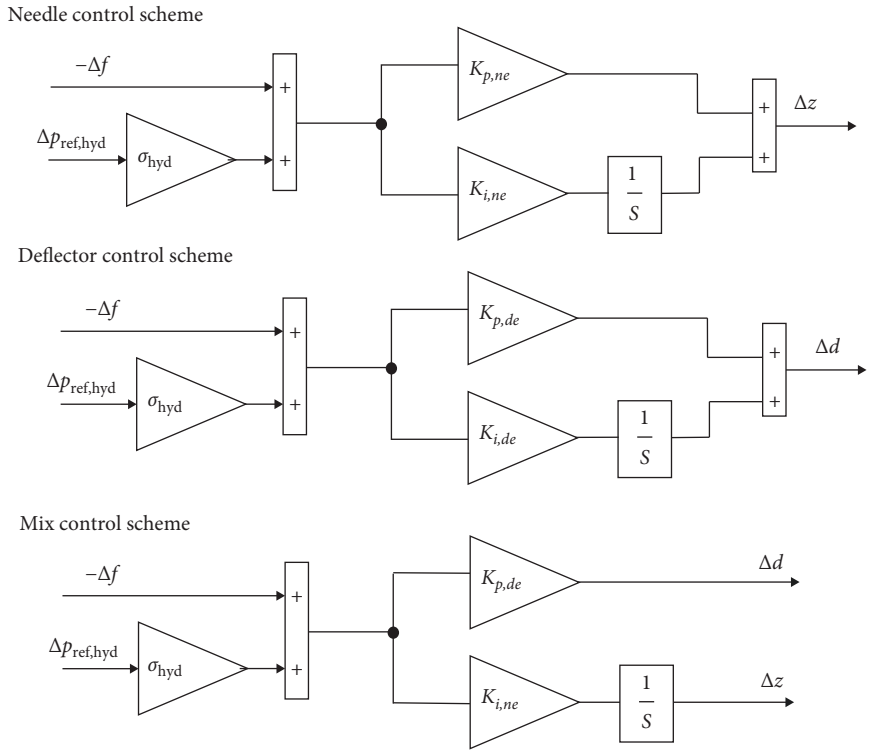


FIGURE 3: Block diagram of the proposed controllers.

$$c_i = q_i\left(2\sqrt{h}\right). \tag{15}$$

However, this expression is valid in cases where the total flow out of the injector impinges on the turbine cups, that is, when the action of the deflector is not taken into account. Therefore, if the regulation capacity of the deflector is to be used, it is necessary to distinguish the flow through the penstock and out of the injector $q$ from the flow that finally hits the turbine runner $q_p$. The relationship between the two flow rates is defined by the deflector opening level $d$, also in p.u. values, as shown in Equation (16), analogous to the model developed by Polster et al. [33]. The parameter $d_i$ takes the value 1 when the deflector does not touch the water jet, while it takes the value 0 when it deflects all the flow completely.

$$q_{p,i} = q_i \cdot d_i. \tag{16}$$

The subscript $i$ refers to each of the four connected Pelton turbines. It follows that, if the deflector is moved, it is satisfied that $d_i < 1$, and therefore the relationship $q_{p,i} < q_i$ is also fulfilled. This means that part of the flow through the penstock does not reach the turbine cups and is therefore wasted. For example, $d_i = 0.9$ implies that the flow out of the injector impinging on the turbine cups (i.e., the turbine flow rate) represents 90% of the total flow through the penstock and, therefore, there is a loss of water equivalent to 10% of this flow.

Subsequently, it is necessary to reformulate Equation (15), which provides the turbine shaft torque, by considering the flow that effectively impacts the turbine runner cups, as expressed in Equation (16). This leads to the actual expression for the torque, given by the following Equation (17), when the deflector is in use.

$$c_i = q_i \cdot d_i \cdot \left(2\sqrt{h}\right). \tag{17}$$

## 3. Proposed Frequency Control Schemes

As described in Section 1, Pelton turbines have two electromechanical elements that can modify the flow of water impinging on the runner. These are the injector needle, which regulates the flow rate of the penstock, and the deflector, which deflects the water jet impinging on the runner and modifies the flow rate impinging on the runner. Thus, it is possible to establish control schemes on both elements as shown in Figure 3 and as described below.

Obviously, many control strategies involving both regulatory elements can be proposed. However, priority has been given to the ease of implementation of the new controllers by adopting an architecture similar to the existing PI controller, which is described in Section 3.1 as the "needle control scheme."

*3.1. Needle Control Scheme.* The governor model of the hydroelectric units used in this study is formulated as indicated in Equation (18), and it is based on [57]. This controller monitors both system frequency and load through feedback signals from the frequency error and power variation. The control loop incorporates the measured frequency system error $(\Delta f)$ as well as the hydroelectric power reference provided $(\Delta p_{\text{ref,hyd}})$ by the

AGC. The governor's action enables the correction of power-frequency errors in response to electrical load variations. The error signal is processed by a conventional PI controller, resulting in an adjustment of the nozzle position ($\Delta z$). The model takes into account both the limits on gate position and its rate of change. This control scheme is the one traditionally used in all Pelton units, and it has been considered in this work in order to compare the results of the new proposed schemes with the usual practice. The main problem with this control scheme is that the movements of the injector needle produce important pressure variations that are transmitted to the generated power, and therefore make frequency control difficult.

$$\Delta z_i = \left[K_{p,ne} + K_{i,ne}\int dt\right]\left(-\Delta f + \sigma_{\text{hyd}} \cdot \Delta p_{\text{ref,hyd}}\right). \quad (18)$$

The variables $K_{p,ne}$ and $K_{i,ne}$ represent the proportional and integral gains of the PI controller, respectively. The mechanical power of the turbine is modified by the increase or decrease of the flow rate to the turbine due to the actuation of the injector needle. Note that, in this control scheme, the deflector is continuously fully open, so the condition that $d_i = 1$ is satisfied.

*3.2. Deflector Control Scheme.* The control carried out by the Pelton turbine deflector is similar to the control carried out by the injector needle, except for the electromechanical element in charge of the control. In this case, the PI controller monitors the same power-frequency error described in the previous section, but it acts on the position of the turbine deflector ($\Delta d$), which is responsible for deflecting the water jet over the turbine, as it is formulated in Equation (19). In fact, with this control scheme, the injector needle is completely open and immobile (i.e., $z_i = 1$ and $d_i < 1$). This control scheme implies that the flow out of the pipe is the maximum, but a part of it is lost and not used to produce energy.

$$\Delta d_i = \left[K_{p,de} + K_{i,de}\int dt\right]\left(-\Delta f + \sigma_{\text{hyd}} \cdot \Delta p_{\text{ref,hyd}}\right). \quad (19)$$

The variables $K_{p,de}$ and $K_{i,de}$ represent the proportional and integral gains of the PI controller, respectively. The mechanical power of the turbine is modified by the variation of the flow impinging on the turbine by the operation of the deflector, without changing the flow through the penstock. In contrast to the traditional "needle control scheme" described in Section 3.1, this one can be much faster because the flow in the penstock is constant, and the regulation does not cause changes in the penstock pressure.

*3.3. Mix Control Scheme.* The proposed mixed control consists of distributing the frequency control effort carried out by the hydroelectric unit between the two electromechanical elements of the turbine. This controller is based on the hierarchical frequency control implemented in many power systems, divided into primary and secondary regulation. In such systems, after a frequency disturbance, primary control acts proportionally to the frequency deviation. This control action must be very fast in order to halt the growing error. Subsequently, secondary control, much slower in response, relieves the primary control action and restores the frequency to its nominal value through an integral controller.

A similar scheme is adopted by variable-speed wind turbines when providing synthetic inertia. This synthetic inertia is based on a proportional control that evaluates the frequency deviation and rapidly adjusts the injected electrical power independently of the available wind power, by leveraging the kinetic energy stored in the rotor, which results in a variation in rotor speed. This speed variation is then slowly corrected by an integral controller that restores the turbine's speed once the system frequency has recovered.

This hierarchical control strategy has been transferred to Pelton units. On the one hand, it is proposed that the deflector reacts by deflecting the water jet proportionally to the measured power frequency error, as shown in Equation (20), analogously to primary control or wind turbine synthetic inertia control. In this way, the deflector's deviation of the jet of water allows rapid action to be taken after the occurrence of the frequency imbalance. The advantage is that this rapid power correction does not cause pressure fluctuations in the pipe, as the flow rate of the pipe is not changed.

$$\Delta d_i = K_{p,de} \cdot \left(-\Delta f + \sigma_{\text{hyd}} \cdot \Delta p_{\text{ref,hyd}}\right). \quad (20)$$

Note that, in this control scheme, the initial reference position of the deflector ($d_0$) must be defined, which must be less than one ($d_0 < 1$) since the turbine must be allowed to increase the power supplied due to the movement of the deflector. This strategy is similar to the concept of "spinning reserve" of a generator; however, in the case of the Pelton turbine, an electrical power lower than the nominal power is not being supplied, but rather a certain flow is being discharged in so that, if necessary, it can be turbined due to the movement of the distributor increasing the power supplied by the turbine. For example, the controller may be configured to have a margin of 5, 10, or 15%… depending on whether the initial position of the deflector is $d_0 = 0.95$, $d_0 = 0.9$, or $d_0 = 0.85$, respectively. It follows that the further away the initial position of the distributor ($d_0$) is from the total aperture ($d_0 = 1$), the greater the wasted flow, but the greater the regulation capacity.

On the other hand, an integral action must be included to correct the steady-state frequency error that the proportional control is not able to correct, which is provided by the turbine injector, as shown in Equation (21), analogously to secondary frequency regulation or wind turbine rotor speed restoration control. In this way, these small and slow corrections do modify the flow rate through the penstock, but in a smoother way, which smooths out the possible pressure oscillations of the penstock.

$$\Delta z_i = K_{i,ne}\int \left(-\Delta f + \sigma_{\text{hyd}} \cdot \Delta p_{\text{ref,hyd}}\right) dt. \quad (21)$$

Although a dual PI control scheme, one for each actuator, could potentially replicate this behavior, such an approach would require an external supervisory controller to coordinate

Table 3: Initial power in simulations.

| Pelton turbines | Wind power plant | Fix speed pumps | Variable speed pumps | Demand |
|---|---|---|---|---|
| 4 × 1.50 MW | 5 × 1.50 MW | 6 × 0.50 MW | 2 × 1.50 MW | 7.50 MW |

the distribution of frequency error and prevent mutual interference between loops. Given these constraints, the control architecture proposed in this work offers a simpler yet effective solution. Nevertheless, the implementation of a coordinated dual PI strategy remains a promising direction for future research, with potential benefits in terms of energy efficiency and dynamic control performance.

## 4. Case Study: El Hierro Island

To test the operation and performance of the new control strategies for Pelton turbines proposed in the previous section, the isolated electricity system of the island of El Hierro, belonging to the Canary archipelago in Spain, is modeled. This system is powered by the Gorona del Viento power plant: a hybrid system with five wind turbines of 2.3 MW each; four Pelton turbines of 2.83 MW; and eight pumps; six of them of 0.5 MW (FST) and two of them of 1.5 MW equipped with power electronics so that they can vary their operating point (VSP). The system also has a power plant with nine diesel units with a total power of 14.94 MW. The island's electricity demand has a peak value of 8.6 MW. Over the last few years, the system has managed to run for many hours on 100% RES. Frequency control, when dispensing with diesel generation, that is, in 100% RES scenarios, presents enormous difficulties as shown in [40]. Frequency control in these cases is performed by Pelton units together with VSP. Wind turbines do not participate in the regulation. In other words, the pumped storage hydroelectric power plant, in order to guarantee the stability of the system, operates under the so-called hydraulic short-circuit, turbining and pumping at the same time, which means a considerable loss in the efficiency of the installation. The capacity to handle the frequency regulation of the pumped storage power plant is not sufficient, as shown in [40]. The length of the penstock is long, so that the inertia of the water limits the speed of response of the Pelton turbine needles. Therefore, as a complementary action, it is also necessary to limit the power of the wind turbines so that wind variability does not affect wind power and, therefore, the frequency. In order to achieve the set objectives and to test how new operating strategies can improve frequency control and overall system performance, two different simulations of the model are considered. The most important numerical characteristics of the dynamic model are shown in [28]. First, the dynamic response of the system is obtained for a situation with variable wind and second, the accidental electrical disconnection of one of the wind turbines, that is, the generator set with the highest connected power, is simulated. In this case, it is assumed that the wind speed (and, therefore, the power of the wind turbines) is constant. Each of the simulations has been carried out for a given combination of initial powers of the Pelton units, wind turbines, pumps, and demand shown in Table 3.

In order to be able to analyze numerically and graphically the effect of the new control strategies, the two simulations are carried out in the following cases:

- Base scenario: Pelton units perform the frequency regulation in the conventional way, that is, by means of the needles.
- Limited wind power: The limitation is introduced in the wind power plant, following the usual practices in the plant. Three maximum powers are proposed for the wind power plant: 7.5, 7.0, and 6.5 MW. The maximum power of wind turbines is 11.5 MW. In this scenario, regulation is carried out by the injector.
- Deflector control: The needles remain completely open, and the frequency control is carried out by the movements of the deflector. In this case, there is no need to limit the power of the wind turbines.
- Mixed control: This is the control scheme resulting from the joint action of needles and deflectors. Three possible initial openings of the deflector ($d_0$) are proposed, 95%, 90% and 85%, so that the smaller the initial opening, the greater the regulation capacity. In this simulation scenario, the power of the wind power plant is not limited.

Figure 4 shows the wind speed record used to simulate the system response for variable wind power conditions. This wind signal was recorded at the plant itself in March 2019.

In order to numerically evaluate the results obtained during simulation with variable wind, applied to the scenarios described above, attention is paid to the frequency, the energy balance, and the efficiency of the system, and, finally, to the wear of the mechanical parts in charge of controlling the flow and therefore the power in the turbines, that is, the needles and deflectors. With respect to the frequency, the maximum and minimum values throughout the simulation (CENIT and NADIR, respectively), the mean square error of the frequency (MSE), and the time in which the frequency remains outside the range $50 \pm 250 \cdot 10^{-3}$ Hz have been measured. From the performance point of view, the energy supplied or consumed by each technology, turbination, pumping, and wind turbines, is measured. The total volume of pumped and turbined water in the pumped storage power plant is also presented, as well as the difference between the two, which determines the overall water balance. Finally, to evaluate the wear of the mechanical regulating elements, the sum of the total movements of the needle and the deflector of the Pelton turbines throughout the simulation is measured according to Yang et al. [58]. Table 4 shows these measured variables under the varying wind conditions of Figure 4 for each scenario.

The numerical and graphical results of the base scenario when simulating a variable wind signal, presented in the first

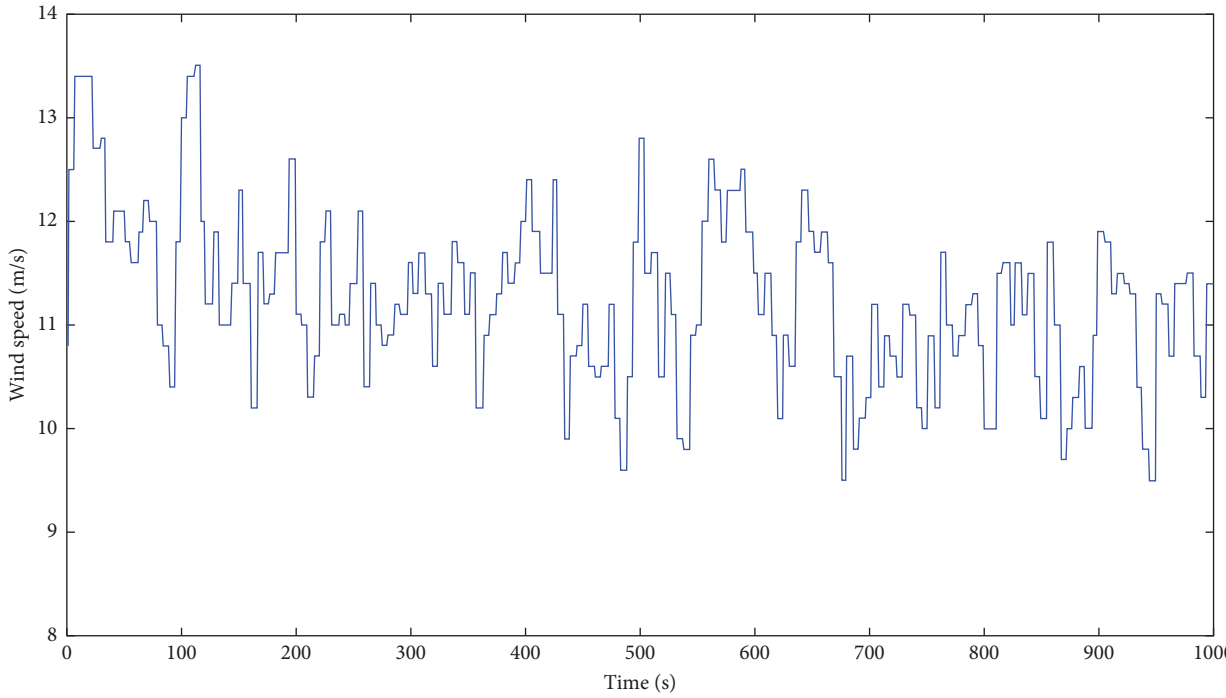


FIGURE 4: Wind speed signal.

TABLE 4: Simulation numerical results assuming a speed signal in the different scenarios.

| Variable | Base | Scenario | | | | | | |
|---|---|---|---|---|---|---|---|---|
| | | Limited wind power to: | | | Deflector | Mix control: $d_0$ | | |
| | | 7.5 MW | 7.0 MW | 6.5 MW | | 0.95 | 0.9 | 0.85 |
| NADIR (Hz) | 47.82 | 48.81 | 49.07 | 49.37 | 49.68 | 49.33 | 49.36 | 49.46 |
| CENIT (Hz) | 53.13 | 51.56 | 51.05 | 50.63 | 50.34 | 50.50 | 50.48 | 50.47 |
| MSE ($Hz^2$) | 0.797 | 0.140 | 0.071 | 0.042 | 0.015 | 0.042 | 0.037 | 0.035 |
| $t_{250}$ (s) | 718.9 | 326.5 | 269.6 | 214.0 | 49.3 | 231.7 | 206.36 | 204.7 |
| $E_{\text{hyd}}$ (MWh) | 1.50 | 1.67 | 1.75 | 1.84 | 1.60 | 1.57 | 1.58 | 1.58 |
| $E_w$ (MWh) | 1.94 | 1.78 | 1.70 | 1.60 | 1.94 | 1.94 | 1.94 | 1.94 |
| $E_{\text{PS}}$ (MWh) | −1.31 | −1.32 | −1.32 | −1.31 | −1.42 | 1.39 | 1.39 | 1.39 |
| $E_{\text{DEM}}$ (MWh) | 2.13 | 2.13 | 2.13 | 2.13 | 2.13 | 2.13 | 2.13 | 2.13 |
| $Vol_{\text{hyd}}$ ($m^3$) | 941.6 | 1049.8 | 1099.1 | 1159.0 | 1794.0 | 1061.0 | 1104.9 | 1163.1 |
| $Vol_{\text{PS}}$ ($m^3$) | −541.9 | −542.1 | −537.6 | −534.0 | −591.8 | 577.0 | 577.6 | 578.3 |
| Balance ($m^3$) | 399.7 | 507.7 | 561.5 | 625.0 | 1201.2 | 484.0 | 527.3 | 584.8 |
| $\int \Delta(z)$ (p.u.) | 8.194 | 3.269 | 2.515 | 2.025 | 0.000 | 1.678 | 1.486 | 1.399 |
| $\int \Delta(d)$ (p.u.) | 0.000 | 0.000 | 0.000 | 0.000 | 7.617 | 6.850 | 7.846 | 8.505 |

column of Table 4 and in Figure 5, respectively, show that this frequency control requires improvements. Currently, wind turbine power is limited in order to reduce wind power variability and, consequently, frequency fluctuations. Columns 2, 3, and 4 of Table 4 and Figure 6 show how limiting the wind power plant output to 7.5, 7.0, and 6.5 MW progressively improves the dynamic behavior of the system frequency. Clearly, this results in a loss of system efficiency, as the unused wind energy prevents pumping a greater amount of water. Fully opening the injectors and controlling hydraulic power through the deflector (deflector control scenario) is an option that works very well in terms of frequency control, as shown in column 5 of Table 4 and in Figures 7 and 8. However, this control strategy involves a very high loss of efficiency, as indicated by the hydraulic balance. Finally, the results obtained with the mixed control strategy, using both injector and deflector on each turbine, are presented in the last columns of Table 4 and in Figure 8, for different initial deflector openings (0.95, 0.90, and 0.85). The results show frequency control similar to that achieved by limiting the wind power, but with improved system efficiency. The wear of the moving parts of the injectors is also reduced, but at the cost of introducing movements of the deflectors. A detailed and comparative analysis of the different scenarios is presented below.

The numerical results obtained from the variable wind simulation in the base scenario show that the frequency control

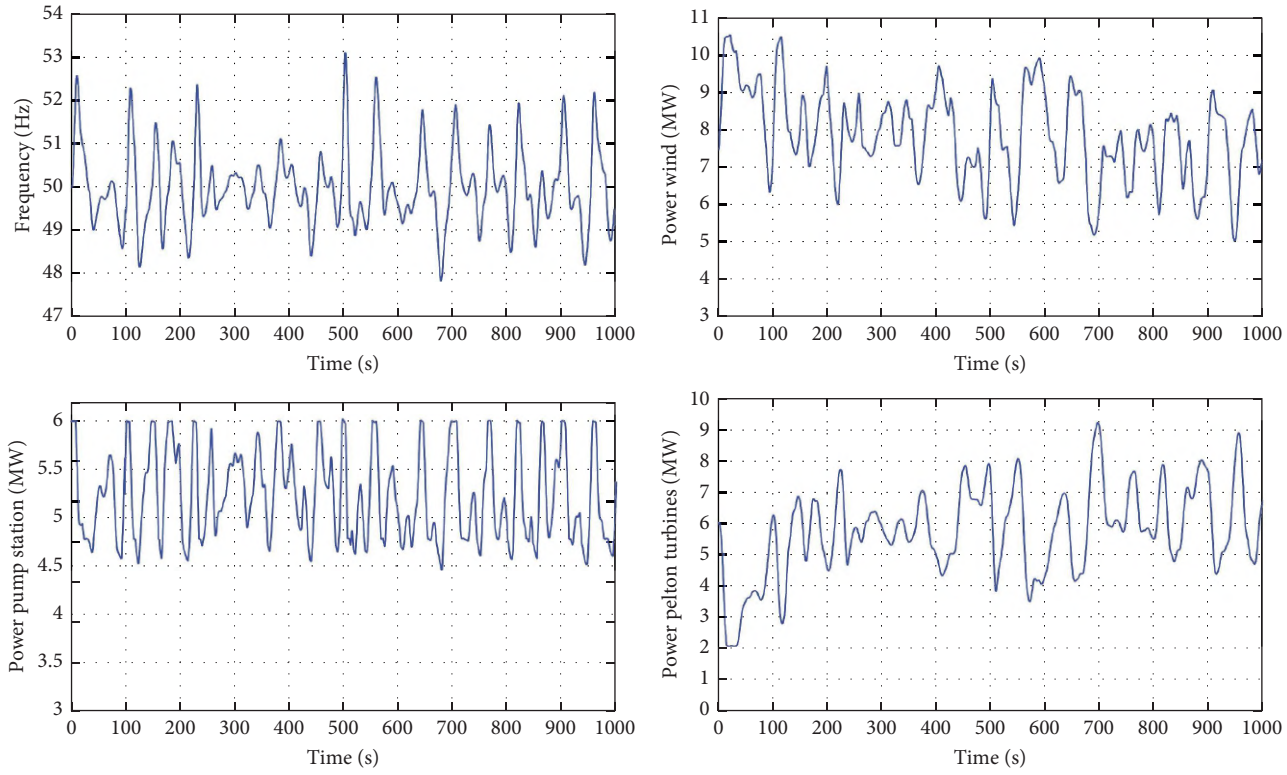


Figure 5: Dynamic response of the system (frequency, wind power, power consumed by the pumps, and power generated by the Pelton turbines) when Pelton units provide frequency regulation conventionally.

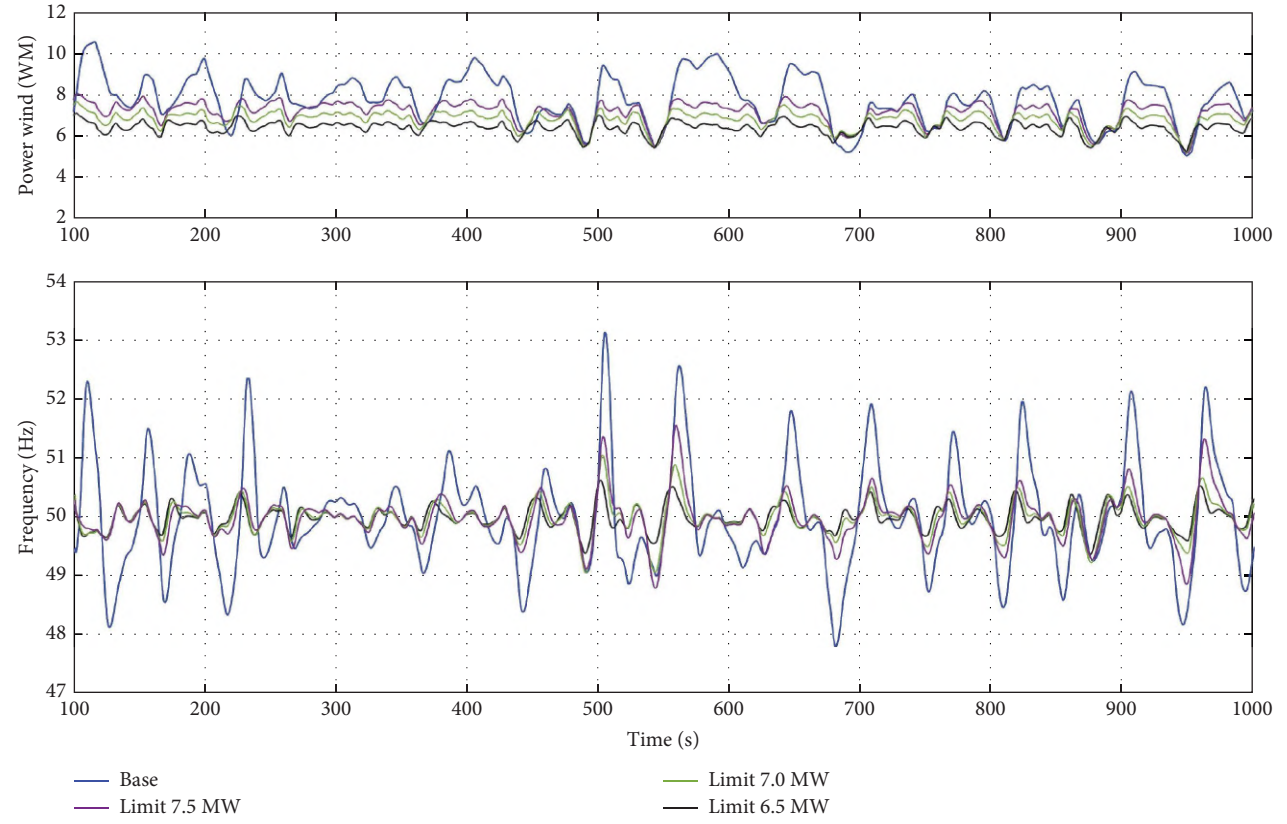


Figure 6: Wind power injected into the power system without power limitation (base case) and with the limitations of 7.5, 7.0, and 6.5 MW, and frequency fluctuations due to this wind power when Pelton units provide frequency regulation conventionally.

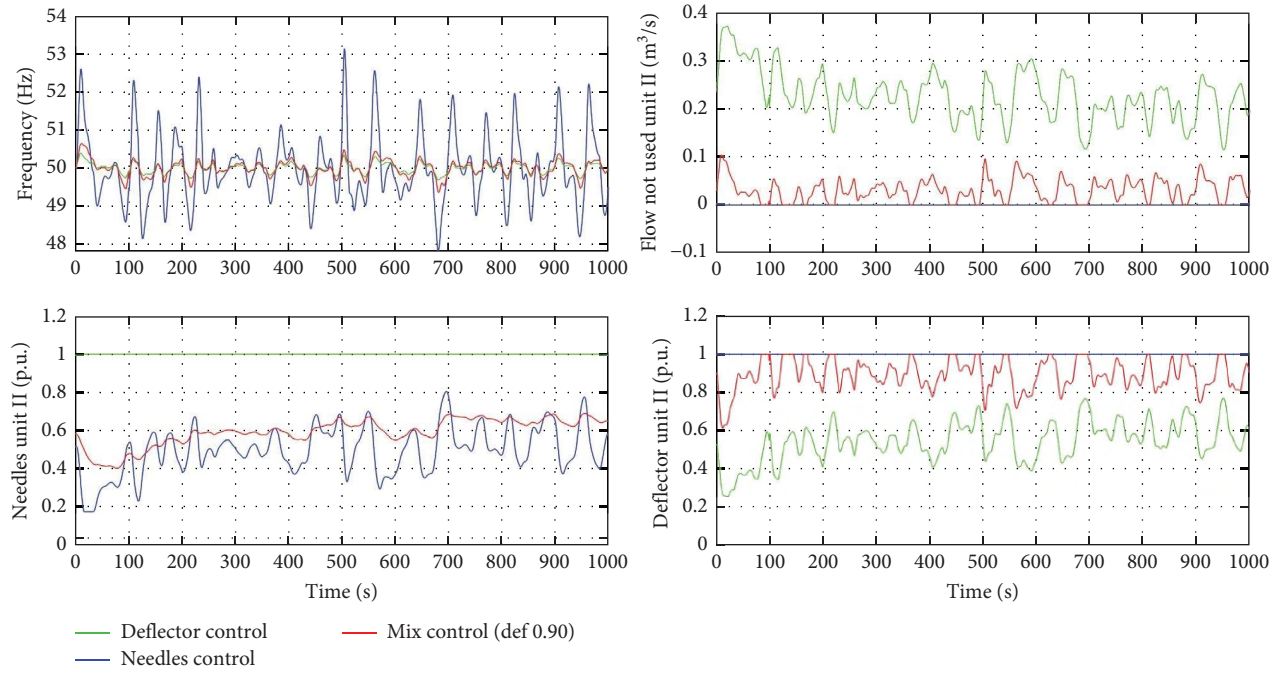


FIGURE 7: Power system frequency and wasted flow, needle opening, and deflector position in the Pelton turbine considering proposed control schemes.

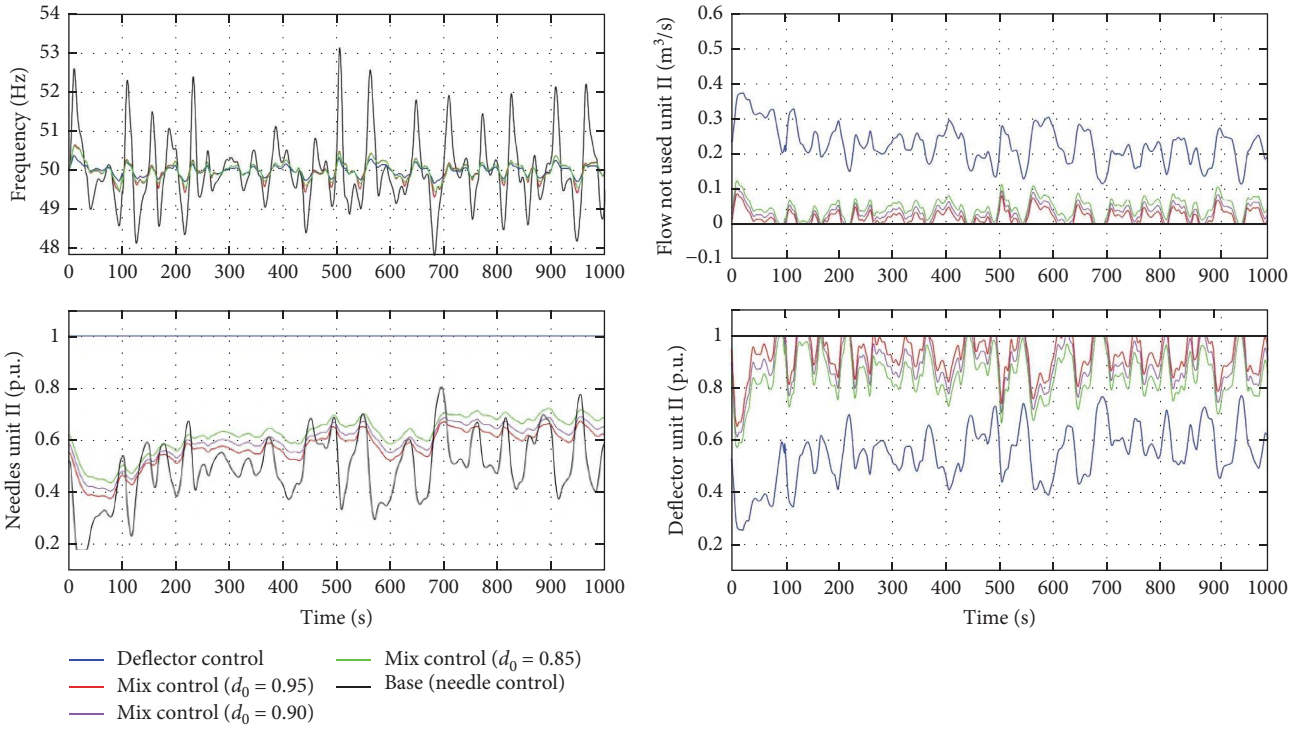


FIGURE 8: Power system frequency and wasted flow, needle opening, and deflector position in the Pelton turbine, considering proposed control schemes, comparing different $d_0$ values.

performed by the Pelton turbines and the VSP is not sufficient. The NADIR reaches a value below 48.0 Hz. This frequency behavior would have triggered the unmodelled load shedding scheme, which would cause the 500 kW pumps to shut down when the frequency drops below 48.9 Hz. Figure 5 shows how the Pelton turbines and VSP react to the high variability of the wind power, but this regulatory action does not prevent the frequency from remaining far below 50 Hz for a long time. As

Table 5: Simulation numerical results assuming a wind turbine disconnection in the different scenarios.

| Variable | Base | Scenario | | | | | | |
|---|---|---|---|---|---|---|---|---|
| | | Limited wind power to: | | | | Mix control: $d_0$ | | |
| | | 7.5 MW | 7.0 MW | 6.5 MW | Deflector | 0.95 | 0.9 | 0.85 |
| NADIR (Hz) | 49.45 | 49.45 | 49.45 | 49.45 | 49.82 | 49.69 | 49.78 | 49.79 |
| $T_s$ (s) | 20.1 | 20.1 | 20.1 | 20.1 | 56.8 | 56.4 | 58.8 | 60.2 |

shown in Table 4, the parameter $t_{250}$ reaches 718.9 s. During the 1000 s that the simulation lasts, the hydraulic balance indicates that 399.7 $m^3$ have passed from the upper reservoir to the lower reservoir.

Limiting the wind power of the wind turbines obviously improves the dynamic frequency response of the system. The results get better as the value limiting the total wind power of the wind power plant is reduced. Thus, as shown in Table 4, the NADIR reaches 48.81, 49.07, and 49.37 Hz when the power is limited to 7.5, 7.0, and 6.5 MW, respectively. The MSE values show a drastic reduction from 0.797 $Hz^2$ in the base scenario to only 0.042 $Hz^2$ when the wind power is limited to 6.5 MW. The value of $t_{250}$ is also considerably reduced by 70.2% in this case. The improvement in frequency response can also be seen in Figure 6, which shows how the limit on wind power in all three cases has a significant influence on frequency.

The limitation of wind power logically leads to a decrease in the energy provided by the wind power plant, which must be compensated by the Pelton turbines. Wind energy decreases from 1.94 to 1.78, 1.70, and 1.60 MWh, respectively, when its maximum power is limited. This affects the water balance significantly so that the volume flowing from the upper to the lower reservoir increases by 27.0%, 31.9%, and 40.1%, respectively. However, the decrease in the variability of the wind power facilitates the work of the Pelton turbine needles. Thus, for the maximum limitation (6.5 MW), their regulation effort ($\int \Delta z$) is reduced by almost a quarter.

If the control is done exclusively by the deflector, the frequency control improves drastically without the need to limit the wind power. The NADIR does not go below 49.68 Hz while the MSE is reduced to 0.015 $Hz^2$. In this case, only for 49.3 s does the frequency exceed the ±250 mHz limit. Figure 6 shows the comparison between the dynamic frequency response of the base scenario without wind power limitation with the deflector control. The same figure shows how the regulating task of the deflectors is similar to that of the needles in the base scenario. But since their movements do not produce sudden pressure changes in the penstock (water hammer), the frequency control is much more effective. Regarding the maintenance of the control devices, the wear of the Pelton turbine deflectors ($\int \Delta d = 7.617$ p.u.) is similar to that of the needles in the base scenario without wind power limitation ($\int \Delta z = 8.194$ p.u.).

However, the disadvantage of these frequency improvements is a significant loss of energy efficiency. Despite the fact that the wind power is not limited, and the pumped volume is increased, the volume of water passing through the turbines is very high because the needles are fully open throughout the simulation. This results in a three-fold increase in the volume of water lost from the upper reservoir compared to the base scenario (from 399.7 to 1202.2 $m^3$). Figure 7 shows the flow that is diverted by the deflectors and does not hit the Pelton runner of unit II.

Finally, in Table 4, the last columns show the results of the scenarios where mixed frequency control is implemented through the Pelton turbine needles and deflectors together. The numerical frequency results show how the mixed control gives similar results to those obtained by limiting the power of the wind power plant. In particular, the mixed control with a deflector initial position of 0.90 p.u. presents values of NADIR, MSE, or $t_{250}$ very similar to those obtained when the wind power is limited to 6.5 MW. The most important benefit of the mixed control is seen in the water volume balance. While the upper reservoir loses 625.0 $m^3$ of water when wind power is limited to 6.5 MW, in the case of mixed control with $d_0 =$ 0.90 p.u., this volume decreases to 527.3 $m^3$. This represents a reduction of 15.6%. Obviously, the base scenario is the one that offers the best hydraulic balance, but with unacceptable frequency values. Figure 7 shows how the mixed control reduces the flow that is diverted by the deflector compared to the control with the deflector alone.

With regard to the wear of the mechanical devices that carry out the regulation, the joint action means that the work of the needles is considerably reduced. Since the needles are responsible for the integral action of the control, their action is much smoother, as can be seen in Figure 7. Compared to the base scenario, the mixed control reduces the regulation effort of the needles by between 4.9 and 5.8, and compared to the scenario with a limitation of 6.5 MW wind power, for example, the effort is reduced by between 1.2 and 1.4. However, since the mixed control distributes the proportional control to the deflector, which is very demanding, its wear ranges between 6.85 and 8.51 p.u. This fact must be considered by the plant owners when inspecting and maintaining these devices. It should not be forgotten that, initially, these regulating elements were only activated as a safety measure when the plant was shut down.

In the case of the simulation showing the dynamic response of the system after the sudden disconnection of the wind turbine, it is only interesting to pay attention to the frequency records, since the duration of the simulation is very short. In this case, the NADIR and the settling time $T_s$, that is, the time in which the frequency stabilizes, are measured. Table 5 and Figure 9 show the numerical and graphical results obtained after the simulation of the accidental disconnection of one of the wind turbines in the different scenarios. The results obtained in the scenarios with wind power limitation are identical to each other and also identical to those of the base

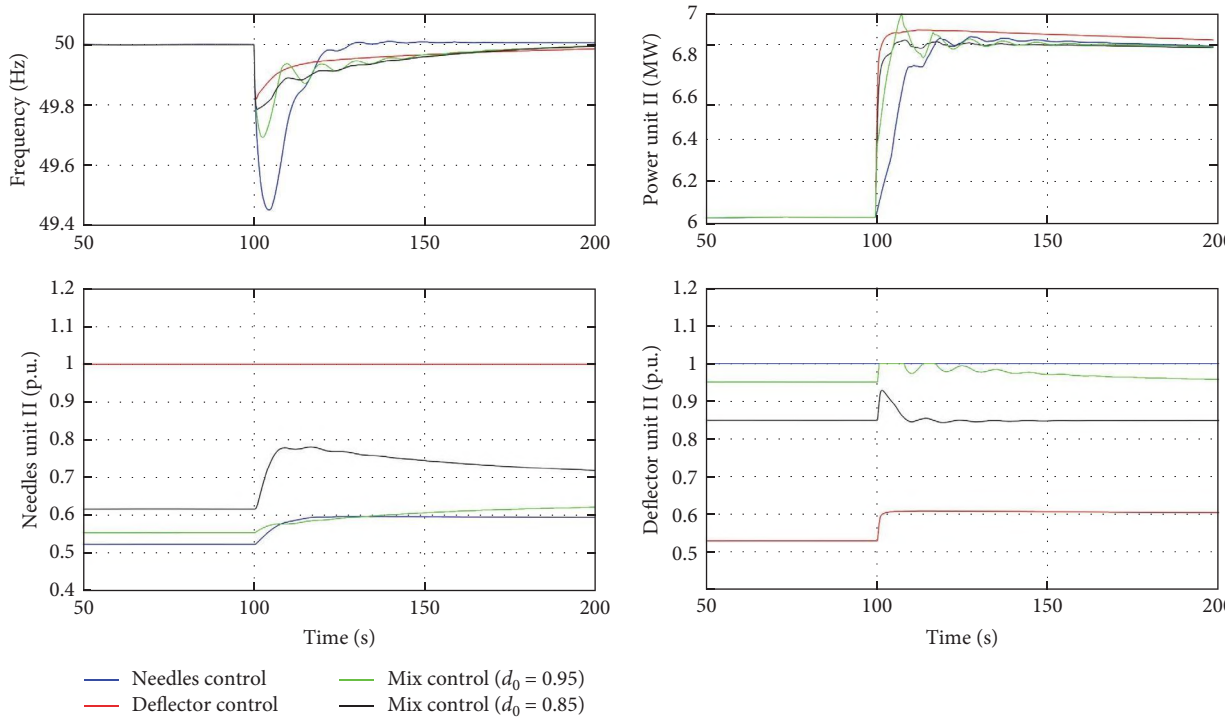


FIGURE 9: System frequency, and power supplied, needle opening, and deflector position in the Pelton turbine after the simulation of the accidental disconnection of one of the wind turbines, assuming different scenarios.

scenario, because in this simulation, the wind speed is constant. Once again, the control carried out exclusively with the deflector is the one that offers the best results. Graphically, it can be seen that the response does not show any trace of oscillation, given that the water hammer in the conduits is completely avoided. In the case of mixed control and initial position of the 0.95 deflector, as shown in Figure 7, the deflector reaches its maximum opening so that its saturated action is limited. This causes the pressure oscillations to be transmitted to the supplied power, as in the base scenario. The action of the deflector in all scenarios, which is much faster than that of the needles, allows the overall system response to be smoothed. This implies an increase in the frequency stabilization time, but at nondamaging values.

Focusing on the energy balance expressed in terms of water volume ($m^3$), the mixed control strategy represents a significant improvement over the current practice of limiting wind power for limiting frequency deviations. To quantitatively assess this saving, for instance, two scenarios with similar frequency performance are compared. The scenario with a 6.5 MW wind power limitation exhibits a minimum NADIR of 49.37 Hz, an MSE of 0.042 $Hz^2$, and a $t_{250}$ of 214.0 s, while the mixed control scenario with an initial deflector opening ($d_0$) of 0.95 shows a minimum NADIR of 49.33 Hz, an MSE of 0.042 $Hz^2$, and a $t_{250}$ of 231.7 s. Wind power limitation results in a water loss from the upper reservoir of 625.0 $m^3$, whereas in the mixed control case, the loss is reduced to 484.0 $m^3$ (22.6% reduction).

Injector actuation is also positively impacted by the mixed control. In the 6.5 MW wind-limitation scenario, the cumulative injector movement amounts to 2.025 p.u., compared to 1.678 p.u. in the mixed control scenario with $d_0 = 0.95$, representing a 17.1% reduction. The only drawback of the mixed control approach is the wear associated with continuous deflector movement, which totals 6.850 p.u., whereas in the wind-limitation scenario, deflector movements are null. Naturally, this wear should be incorporated into the turbines' maintenance planning, as previously mentioned.

As a future line of research, it would be of interest to monetize all these aspects and economically quantify the improvements that this new control strategy could bring to El Hierro's electrical system.

## 5. Conclusions

This study addresses the challenges of frequency regulation in isolated power systems with high renewable energy integration, using El Hierro Island as a case study. It highlights the limitations of traditional needle-based control in Pelton turbines and explores alternative strategies, including the deflector of the turbines, to enhance stability and efficiency. Traditional needle-based control showed poor frequency stability, reaching unacceptable values, and making it necessary to limit the wind power generation. In that case, limiting the wind power improved the frequency stability to admissible values, but it sacrificed renewable energy utilization (up to 40% of the wind energy was unused). The proposed deflector-based control significantly enhanced stability without limiting wind power. In fact, it achieved the best frequency stability, but it entailed tripling the volume of water coming from the upper reservoir to generate the same energy, with the consequent water loss. The mixed control scheme, combining needles and deflectors, offered the best

balance, as it reduced the frequency deviations, minimized water loss, and improved overall system performance compared to the traditional needle-based control with wind power limitation. These findings demonstrate the potential of advanced control methods to maximize renewable energy integration while maintaining operational resilience in isolated systems.

## Nomenclature

$A_r$: Area swept by rotor blades ($m^2$)
AGC: Automatic generation control
$\beta$: VSWT blade pitch angle (°)
$c$: Shaft torque of the Pelton turbine (p.u.)
$c_{h,i}$, $b_{h,i}$, $a_{h,i}$: Coefficients of pump characteristic function
$c_{p,i}$, $b_{p,i}$, $a_{p,i}$: Coefficients of pump characteristic function
CENIT: Maximum frequency value
$C_p$: VSWT power coefficient
$d$: Deflector opening level of the Pelton turbine (p.u.)
$d_0$: Initial deflector opening level of the Pelton turbine (p.u.)
$\Delta d$: Variation of the deflector position (p.u.)
$\Delta f$: System frequency error (p.u.)
$\Delta p_{\text{ref,hyd}}$: Hydroelectric power reference variation (p.u.)
$\Delta RR$: Total secondary regulation effort
$\Delta z$: Variation of the nozzle position (p.u.)
$D_{\text{net}}$: Sensitivity of consumer load to frequency deviation (p.u.)
$E_{\text{DEM}}$: Energy demand (MWh)
$E_{\text{hyd}}$: Energy provided by the hydroelectric units (MWh)
$E_{\text{PS}}$: Energy consumed by the pump station (MWh)
$E_w$: Energy provided by the wind turbines (MWh)
$f$: System frequency (p.u.)
$g$: Gravity acceleration ($m/s^2$)
$H_b$: Base head (m)
$H_{\text{hyd}}$: Inertia constant of the hydroelectric units (s)
$H_\omega$: Wind turbine inertia constant (s)
$h$: Net head of the hydroelectric units (p.u.)
$h_m$: Net head (p.u.)
$h_{n,i}$: Pumped head by each pump (p.u.)
$i$: Online Pelton turbine number
$J_i$: Rotor pump inertia (s)
$K_f$: $K$-factor in the control area (MW/Hz)
$K_{i,de}$: Integral gain of the PI controller of the deflector control
$K_{i,ne}$: Integral gain of the PI controller of the nozzle control
$K_{i,\omega}$: Integral gain in PI VSWT speed control
$K_{p,de}$: Proportional gain of the PI controller of the deflector control
$K_{p,ne}$: Proportional gain of the PI controller of the nozzle control
$K_{p,i}$: Pump integral gain
$K_{p,p}$: Pump proportional gain
$K_{p,\omega}$: Proportional gain in PI VSWT speed control
$K_{u,i}$: Synchronized generating unit participation factors
$\lambda$: Ratio of rotor blade tip speed to wind speed
$L$: Penstock length (m)
MSE: Mean square error of the frequency ($Hz^2$)
$n_{\text{nom},i}$: Nominal rotational speed of each pump (p.u.)
$n_p$, $i$: Rotational speed of each pump (p.u.)
$n_t$: Number of segments of the penstock
$N_{\text{syn}}$: Synchronous speed (r.p.m.)
NADIR: Minimum frequency value (Hz)
$p_{e,i}$: Power consumed by each pump (p.u.)
$p_{\text{fsp}}$: Power consumed by fixed speed pumps (p.u.)
$p_{\text{hyd}}$: Power supplied by hydroelectric units (p.u.)
$p_{\text{nc}}$: Power supplied by VSWT converter (p.u.)
$p_\omega$: Power reference provided by VSWT speed control (p.u.)
$p_{p,i}$: Mechanical power of each pump (p.u.)
$p_{\text{vsp}}$: Power consumed by variable speed pumps (p.u.)
$p_w$: Power supplied by wind turbines (p.u.)
$P_w$: Power supplied by wind turbines (MW)
$P_{\text{wind}}$: Wind mechanical power (MW)
PI: Proportional-integral
$q$: Flow of the hydroelectric unit (p.u.)
$q_{p,m}$: Flow pumped by each pump (p.u.)
$Q_b$: Base flow in the penstock ($m^3/s$)
RES: Renewable energy source
$\rho$: Air density: 1.225 $kg/m^3$ ($kg/m^3$)
$r/2$: Continuous head losses coefficient in the penstock (p.u.)
$s_{\text{nom}}$: Electrical machine slip (p.u.)
$s_w$: Wind speed (m/s)
$S$: Penstock cross-sectional area ($m^2$)
$T_e$: Elastic time ($=$ L/a) (s)
$T_s$: Settling time (s)
$T_{u,i}$: Time constant of the AGC system for each generation unit $i$ (s)
$T_w$: Penstock water starting time (s)
$t_{250}$: Time frequency is outside ±250 mHz limits (s)
$Vol_{\text{hyd}}$: Turbined water volume ($m^3$)
$Vol_{PS}$: Pumped water volume ($m^3$)
vRES: Variable renewable energy source
$\omega$: VSWT rotational rotor speed (p.u.)
$z$: Nozzle opening of the hydroelectric units (p.u.)
$\Delta z$: Variation of the nozzle position (p.u.)
$\sigma_{\text{hyd}}$: Hydro units speed droop (p.u.).

## Data Availability Statement

The data are available upon request from the authors.

## Conflicts of Interest

The authors declare no conflicts of interest.

## Funding

This study was supported by the Ministerio de Ciencia, Innovación y Universidades (Grant PID2021-126082OB-C22); the Ministerio de Economía y Competitividad (Grant ENE2016-77951-R); and the Madrid Government (Comunidad de Madrid-Spain) under the Multiannual Agreement 2023-2026 with Universidad Politécnica de Madrid in the Line A, Emerging PhD researchers, under Grant DOCTORES-EMERGENTES-24-Y8X7NY-18-RPLBQC.

## Acknowledgments

The authors thank Gorona del Viento El Hierro, S.A. for the data provided.

## References

[1] Z. Ullah, G. Mokryani, F. Campean, and Y. F. Hu, "Comprehensive Review of VPPs Planning, Operation and Scheduling Considering the Uncertainties Related to Renewable Energy Sources," *IET Energy Systems Integration* 1, no. 3 (2019): 147–157.

[2] A. Fernández-Guillamón, J. I. Sarasúa, M. Chazarra, A. Vigueras-Rodríguez, D. Fernández-Muñoz, and Á. Molina-García, "Frequency Control Analysis Based on Unit Commitment Schemes With High Wind Power Integration: A Spanish Isolated Power System Case Study," *International Journal of Electrical Power & Energy Systems* 121 (2020): 106044.

[3] G. Msigwa, J. O. Ighalo, and P.-S. Yap, "Considerations on Environmental, Economic, and Energy Impacts of Wind Energy Generation: Projections Towards Sustainability Initiatives," *Science of the Total Environment* 849 (2022): 157755.

[4] A. Fernández-Guillamón, A. Vigueras-Rodríguez, and Á. Molina-García, "Analysis of Power System Inertia Estimation in High Wind Power Plant Integration Scenarios," *IET Renewable Power Generation* 13, no. 15 (2019): 2807–2816.

[5] K. S. Ratnam, K. Palanisamy, and G. Yang, "Future Low-Inertia Power Systems: Requirements, Issues, and Solutions—A Review," *Renewable and Sustainable Energy Reviews* 124 (2020): 109773.

[6] J. H. Zhang, L. Y. Liu, Y. Q. Liu, Y. R. Zhu, and J. Yan, "Research on Robust Model Predictive Control Strategy of Wind Turbines to Reduce Wind Power Fluctuation," *Electric Power Systems Research* 213 (2022): 108809.

[7] O. Erdinc, N. G. Paterakis, and J. P. S. Catalão, "Overview of Insular Power Systems Under Increasing Penetration of Renewable Energy Sources: Opportunities and Challenges," *Renewable and Sustainable Energy Reviews* 52 (2015): 333–346.

[8] E. Semshchikov, M. Negnevitsky, J. Hamilton, and X. Wang, "Cost-Efficient Strategy for High Renewable Energy Penetration in Isolated Power Systems," *IEEE Transactions on Power Systems* 35, no. 5 (2020): 3719–3728.

[9] I. Egido, L. Sigrist, E. Lobato, et al., "Energy Storage Systems for Frequency Stability Enhancement in Small-Isolated Power Systems," *Energy* 13 (2015): 820–825.

[10] G. M. de Lucas, *Frequency Control of Hybrid Wind-Hydro Power Plants With Long-Term Energy Storage*, (PhD thesis, Universidad Politécnica de Madrid, 2018).

[11] J. Machowski, Z. Lubosny, J. W. Bialek, and J. R. Bumby, *Power System Dynamics: Stability and Control* (John Wiley & Sons, 2020).

[12] O. M. Babatunde, J. L. Munda, and Y. Hamam, "Power System Flexibility: A Review," *Energy Reports* 6 (2020): 101–106.

[13] R. Vakulchuk, I. Overland, and D. Scholten, "Renewable Energy and Geopolitics: A Review," *Renewable and Sustainable Energy Reviews* 122 (2020): 109547.

[14] F. Hao and W. Shao, "What Really Drives the Deployment of Renewable Energy? A Global Assessment of 118 countries," *Energy Research & Social Science* 72 (2021): 101880.

[15] S. Thapa, T. Magee, and E. Zagona, "Factors That Affect Hydropower Flexibility," *Water* 14, no. 16 (2022): 2563.

[16] S. Rehman, L. M. Al-Hadhrami, and M. M. Alam, "Pumped Hydro Energy Storage System: A Technological Review," *Renewable and Sustainable Energy Reviews* 44 (2015): 586–598.

[17] D. A. Katsaprakakis, D. G. Christakis, K. Pavlopoylos, et al., "Introduction of a Wind Powered Pumped Storage System in the Isolated Insular Power System of Karpathos-Kasos," *Applied Energy* 97 (2012): 38–48.

[18] P. Beires, M. H. Vasconcelos, C. L. Moreira, and J. A. P. Lopes, "Stability of Autonomous Power Systems With Reversible Hydro Power Plants: A Study Case for Large Scale Renewables Integration," *Electric Power Systems Research* 158 (2018): 1–14.

[19] M. H. Vasconcelos, P. Beires, C. L. Moreira, and J. A. P. Lopes, "Dynamic Security of Islanded Power Systems With Pumped Storage Power Plants for High Renewable Integration—A Study Case," *The Journal of Engineering* 2019, no. 18 (2019): 4955–4960.

[20] R. Sebastián and A. Nevado, "Study and Simulation of a Wind Hydro Isolated Microgrid," *Energies* 13, no. 22 (2020): 5937.

[21] Of Eigg Authority TI, Eigg Electric, Accessed on 2 Oct 2024 http://isleofeigg.org/Eigg-Electric/.

[22] J. I. Sarasúa, G. Martínez-Lucas, J. I. Pérez-Díaz, and D. Fernández-Muñoz, "Alternative Operating Modes to Reduce the Load Shedding in the Power System of El Hierro Island," *International Journal of Electrical Power & Energy Systems* 128 (2021): 106755.

[23] M. Egusquiza, E. Egusquiza, C. Valero, A. Presas, D. Valentín, and M. Bossio, "Advanced Condition Monitoring of Pelton Turbines," *Measurement* 119 (2018): 46–55.

[24] S. Bhattarai, P. Vichare, K. Dahal, A. Al Makky, and A. G. Olabi, "Novel Trends in Modelling Techniques of Pelton Turbine Bucket for Increased Renewable Energy Production," *Renewable and Sustainable Energy Reviews* 112 (2019): 87–101.

[25] A. K. Liamasov, K. E. Denisov, and M. A. Biriulin, "A New Method for Regulating Pelton Turbine Based on Ejection of Discharged Flow," *E3S Web of Conferences* 411 (2023): 01047.

[26] G. Martínez-Lucas, J. I. Sarasúa, J. Á. Sánchez-Fernández, and J. R. Wilhelmi, "Power-Frequency Control of Hydropower Plants With Long Penstocks in Isolated Systems With Wind Generation," *Renewable Energy* 83 (2015): 245–255.

[27] G. Martínez-Lucas, J. I. Sarasúa, and J. Á. Sánchez-Fernández, "Frequency Regulation of a Hybrid Wind–Hydro Power Plant in an Isolated Power System," *Energies* 11, no. 1 (2018): 239.

[28] G. Martínez-Lucas, J. I. Sarasua, A. Fernández-Guillamón, and Á. Molina-García, "Combined Hydro-Wind Frequency Control Scheme: Modal Analysis and Isolated Power System Case Example," *Renewable Energy* 180 (2021): 1056–1072.

[29] Z. Zhang, *Pelton Turbines* (Springer, 2016).

[30] R. M. Johnson, J. H. Chow, and M. V. Dillon, "Pelton Turbine Deflector Overspeed Control for a Small Power System," in *2003 IEEE Power Engineering Society General Meeting*, (IEEE, 2003): 2171–2176.

[31] R. M. Johnson, J. H. Chow, and M. V. Dillon, "Pelton Turbine Deflector Overspeed Control for a Small Power System," *IEEE Transactions on Power Systems* 19, no. 2 (2004): 1032–1037.

[32] L. Wang, J. Zhao, D. Liu, et al., "Governor Tuning and Digital Deflector Control of Pelton Turbine With Multiple Needles for Power System Studies," *IET Generation, Transmission & Distribution* 11, no. 13 (2017): 3278–3286.

[33] S. C. Polster, R. Schürhuber, H. R. R. Schmaranz, C. Rupp, and C. Tengg, "Modelling of Black Start and Island Grid Operation With Deflector Controlled Pelton Units," Hydro 2019-Concept to Closure: Practical Steps (2019).

[34] A. Marrero, J. González, J. A. Carta, and P. Cabrera, "A New Control Algorithm to Increase the Stability of Wind–Hydro Power Plants in Isolated Systems: El Hierro as a Case Study," *Journal of Marine Science and Engineering* 11, no. 2 (2023): 335.

[35] T. Wilberforce, E. T. Sayed, M. A. Abdelkareem, M. Mahmoud, and A. G. Olabi, "Development of Hydropower Technology," in *Renewable Energy-Volume 1: Solar, Wind, and Hydropower*, (Elsevier, 2023): 427–450.

[36] Y. V. Makarov, B. Yang, J. G. DeSteese, et al., *Wide-Area Energy Storage and Management System to Balance Intermittent Resources in the Bonneville Power Administration and California ISO Control Areas* (Pacific Northwest National Lab. (PNNL), 2008).

[37] H. Vasconcelos, C. Moreira, A. Madureira, J. P. Lopes, and V. Miranda, "Advanced Control Solutions for Operating Isolated Power Systems: Examining the Portuguese Islands," *IEEE Electrification Magazine* 3, no. 1 (2015): 25–35.

[38] G. Martínez-Lucas, J. I. Sarasúa, and J. Á. Sánchez-Fernández, "Eigen Analysis of Wind–hydro Joint Frequency Regulation in an Isolated Power System," *International Journal of Electrical Power & Energy Systems* 103 (2018): 511–524.

[39] A. Fernández-Guillamón, G. Martínez-Lucas, Á. Molina-García, and J. I. Sarasua, "Hybrid Wind–PV Frequency Control Strategy Under Variable Weather Conditions in Isolated Power Systems," *Sustainability* 12, no. 18 (2020): 7750.

[40] A. M. Quevedo, E. J. M. Domínguez, J. M. de León Izquier, R. C. de León, P. S. Arozarena, J. G. Moreno, et al., "Gorona del Viento Wind-Hydro Power Plant," in *3rd International Hybrid Power Systems Workshop*, (Energynautics GmbH, 2018).

[41] S. P. Mansoor, D. I. Jones, D. A. Bradley, F. C. Aris, and G. R. Jones, "Reproducing Oscillatory Behaviour of a Hydroelectric Power Station by Computer Simulation," *Control Engineering Practice* 8, no. 11 (2000): 1261–1272.

[42] J. I. Sarasúa, G. Martínez-Lucas, and M. Lafoz, "Analysis of Alternative Frequency Control Schemes for Increasing Renewable Energy Penetration in El Hierro Island Power System," *International Journal of Electrical Power & Energy Systems* 113 (2019): 807–823.

[43] J. O'Sullivan, A. Rogers, D. Flynn, P. Smith, A. Mullane, and M. O'Malley, "Studying the Maximum Instantaneous Non-Synchronous Generation in an Island System—Frequency Stability Challenges in Ireland," *IEEE Transactions on Power Systems* 29, no. 6 (2014): 2943–2951.

[44] D. Fernández-Muñoz, J. I. Pérez-Díaz, and M. Chazarra, "A Two-Stage Stochastic Optimisation Model for the Water Value Calculation in a Hybrid Diesel/Wind/Pumped-Storage Power System," *IET Renewable Power Generation* 13, no. 12 (2019): 2156–2165.

[45] J. I. Sarasúa, G. Martínez-Lucas, C. A. Platero, and J. Á. Sánchez-Fernández, "Dual Frequency Regulation in Pumping Mode in a Wind–Hydro Isolated System," *Energies* 11, no. 11 (2018): 2865.

[46] K. Clark, N. W. Miller, and J. J. Sanchez-Gasca, "Modeling of GE Wind Turbine-Generators for Grid Studies," *GE Energy* 4 (2010): 0885–8950.

[47] P. Bhatt, R. Roy, and S. P. Ghoshal, "Dynamic Participation of Doubly Fed Induction Generator in Automatic Generation Control," *Renewable Energy* 36, no. 4 (2011): 1203–1213.

[48] Y. Sun, Z. Zhang, G. Li, and J. Lin, "Review on Frequency Control of Power Systems With Wind Power Penetration," in *2010 International Conference on Power System Technology*, (IEEE, 2010): 1–8.

[49] A. S. Ahmadyar and G. Verbič, "Control Strategy for Optimal Participation of Wind Farms in Primary Frequency Control," in *2015 IEEE Eindhoven PowerTech*, (IEEE, 2015): 1–6.

[50] J. M. Mauricio, A. Marano, A. Gomez-Exposito, and J. L. M. Ramos, "Frequency Regulation Contribution Through Variable-Speed Wind Energy Conversion Systems," *IEEE Transactions on Power Systems* 24, no. 1 (2009): 173–180.

[51] S. Zhao and N.-K. C. Nair, "Assessment of Wind Farm Models From a Transmission System Operator Perspective Using Field Measurements," *IET Renewable Power Generation* 5, no. 6 (2011): 455–464.

[52] J. I. Sarasúa, J. I. Pérez-Díaz, G. Martínez-Lucas, and D. Fernández-Muñoz, "Simplified Event-Based Load Shedding Scheme for Frequency Stability in an Isolated Power System With High Renewable Penetration. El Hierro: A Case Study," *Frontiers in Energy Research* 9 (2021): 698081.

[53] J. I. Pérez-Díaz, J. I. Sarasúa, and J. R. Wilhelmi, "Contribution of a Hydraulic Short-Circuit Pumped-Storage Power Plant to the Load–frequency Regulation of an Isolated Power System," *International Journal of Electrical Power & Energy Systems* 62 (2014): 199–211.

[54] UCTE (Union for the Co-ordination of Transmission of Electricity), "Operation Handbook," 2004, https://www.entsoe.eu/publications/system-operations-reports/operation-handbook.

[55] A. J. Wood, B. F. Wollenberg, and G. B. Sheblé, *Power Generation, Operation, and Control* (John Wiley & Sons, 2013).

[56] W. G. P. Mover and E. Supply, "Hydraulic Turbine and Turbine Control Models for System Dynamic Studies," *IEEE Transactions on Power Systems* 7, no. 1 (1992): 167–179.

[57] J. I. Pérez-Díaz, J. Wilhelmi, I. Galaso, et al., "Dynamic Response of Hydro Power Plants to Load Variations for Providing Secondary Regulation Reserves considering Elastic Water Column Effects," *Energy* 1 (2012): 159–163.

[58] W. Yang, P. Norrlund, L. Saarinen, J. Yang, W. Guo, and W. Zeng, "Wear and Tear on Hydro Power Turbines–Influence From Primary Frequency Control," *Renewable Energy* 87 (2016): 88–95.